Journal of Science: Advanced Materials and Devices 7 (2022) 100394

Contents lists available at ScienceDirect

Journal of Science: Advanced Materials and Devices

journal homepage: www.elsevier.com/locate/jsamd

Original Article

Effect of surface tension and drying time on inkjet-printed PEDOT:PSS for ITO-free OLED devices

Marco Cinquino [a, b], Carmela Tania Prontera [b, *], Alessandra Zizzari [b], Antonella Giuri [b], Marco Pugliese [a, b, **], Roberto Giannuzzi [a, b], Anna Grazia Monteduro [a, b], Matteo Carugati [c], Augusto Banfi [c], Sonia Carallo [b], Aurora Rizzo [b], Antonio Andretta [d], Giovanni Dugnani [c], Giuseppe Gigli [a, b], Vincenzo Maiorano [b]

[a] University of Salento, Department of Mathematics and Physics "Ennio De Giorgi", Via Arnesano, 73100, Lecce, Italy
[b] National Research Council, Institute of Nanotechnology (CNR-NANOTEC), Via Monteroni, 73100, Lecce, Italy
[c] T.P.A. SRL, Via Carducci 221, 20099, Sesto San Giovanni, MI, Italy
[d] Klopman International S.r.l., Via Armando Vona 34, 03100, Frosinone, Italy

ARTICLE INFO

Article history:
Received 4 February 2021
Received in revised form
27 July 2021
Accepted 2 September 2021
Available online 11 September 2021

Keywords:
PEDOT:PSS
Surface tension
Co-solvent
Inkjet printing
Organic light-emitting diodes
ITO-Free

ABSTRACT

Highly conductive PEDOT:PSS is one of the most promising materials for indium tin oxide (ITO) substitution in printed electronics. Here, we report the development and optimisation of two PEDOT:PSS ink formulations for the fabrication of inkjet-printed transparent conductive layers. Starting from aqueous commercial solutions, co-solvents and a non-ionic surfactant were employed to modify the surface tension, improve the wetting capability of the ink, and obtain uniform and homogeneous thin films. In particular, the quantities of ethanol and surfactant were systematically adjusted to determine the optimal conditions for inkjet printing. The results demonstrate that a surface tension value between 28 and 40 mN/m and approximately 40 vol.% of a low-boiling-point co-solvent are fundamental to ensure the proper wetting of the glass substrate and a quick-drying process that confers uniformity to the printed thin film. The printed PEDOT:PSS thin films show good morphological, optical, and electrical properties that are similar to those observed for the corresponding spin-coated layers. The organic light-emitting diodes (OLEDs) fabricated with the inkjet-printed PEDOT:PSS electrodes showed a maximum quantum efficiency of 5.5% and a maximum current efficiency of 15 cd/A, which is comparable to spin-coated reference devices. Our study demonstrates the great potential of polymeric electrodes for the fabrication of high-efficiency printed OLED devices that are compatible with flexible and stretchable substrates.

1. Introduction

Organic electronics is a research field of growing interest because they are a low-cost alternative to traditional electronics in terms of both material costs and manufacturing processes. In this context, organic light-emitting diodes (OLEDs) have emerged as one of the most promising device architectures for solid-state lighting and displays, owing to their various advantages such as light weight, flexibility, high luminous power efficiency, low power consumption, large viewing angle, and cost advantages compared to inorganic devices [1].

Several fabrication techniques can be used to produce such devices; however, contemporary highest quality OLEDs are fabricated through thermal evaporation, which has a high cost and low scalability [1]. Efficient solution-based deposition processes are required to produce large-area electronic devices and reduce

* Corresponding author. National Research Council, Institute of Nanotechnology (CNR-NANOTEC), Via Monteroni, 73100, Lecce, Italy.
** Corresponding author. National Research Council, Institute of Nanotechnology (CNR-NANOTEC), Via Monteroni, 73100, Lecce, Italy.
E-mail addresses: tania.prontera@nanotec.cnr.it (C.T. Prontera), marco.pugliese@nanotec.cnr.it (M. Pugliese).
Peer review under responsibility of Vietnam National University, Hanoi.

https://doi.org/10.1016/j.jsamd.2021.09.001

fabrication costs. In particular, spin-coating [2], dip coating [3], and blade coating [4] processes have been developed, but they have several disadvantages. Such coating technologies involve the wastage or contamination of a large amount of material; furthermore, these types of processes are better suited for small-size applications and are extremely non-specific. In recent years, printing technologies have attracted increasing attention because they can be employed for the fabrication of low-cost and large-area electronic devices using simple and easily scalable additive processing [5]. Specifically, inkjet printing ensures high-resolution and high-speed deposition with minimal material waste [6]. It is a non-contact and mask-free deposition method; therefore, it can be used for the fabrication of multilayer structures without the application of patterning processes [5,6]. During the last decade, significant results have been achieved by printing OLED layers, such as hole injection and emitting layers [7–9], even if the production of efficient fully printed devices is still challenging.

Among the possible printable materials for OLED manu facturing, poly (3,4-ethylenedioxythiophene) polystyrene sulfonate (PEDOT:PSS) is a water-soluble polymer that is widely used both as a hole injection layer and an electrode. In particular, there are numerous papers related to the development of methodologies to improve the conductivity and morphology of PEDOT:PSS thin films for use as transparent conductive electrodes in optoelectronic devices. High boiling point solvents (ethylene glycol (EG) and dimethyl sulfoxide (DMSO)) [10,11], polyethylene glycol (PEG) [12], surfactants [13], and ionic liquids [14] are some examples of additives employed to obtain highly conductive PEDOT:PSS thin films. Moreover, several post-treatments have been developed with the same aim [15,16]. However, most of the formulations developed in the above-mentioned works cannot be used in printing technologies without modification. Indeed, most printing and innovative deposition techniques require specific rheological and surface tension properties to obtain high-quality thin films. PEDOT:PSS formulations for gravure printing [17], spray coating [18], and inkjet printing [9] have already been developed. In particular, the quality of an inkjet-printed thin film is strongly affected by the ink formulation and ink-substrate interactions. The surface tension, viscosity, and solid content of the ink must be modulated to optimise the jetting process [19]. Furthermore, the ink/substrate interface should be evaluated to obtain uniform thin films [19]. When a drop is placed on a surface, there are two opposite behaviours that can occur. High surface tension usually leads to contact line recession and dewetting phenomena [20]; in contrast, when the contact line is pinned on the substrate, the evaporation rate of the drop is greater at its edge and the so-called “coffee ring” effect is observed [21]. Both pinning and contact line recession are two unwanted effects that worsen the uniformity of printed thin films. By modulating the properties of the ink formulation, it is possible to balance the effects and deposit uniform and homogeneous thin films [22].

Inkjet-printed PEDOT:PSS has been developed and reported for various applications, such as stretchable electrical connections and circuits [23], transistors [24], and RC filters [25]. Many studies have been conducted on the inkjet printing of low-conductivity PEDOT:PSS that can act as hole injection and transport layers for use in optoelectronic devices. In 2009, *Eom* et al. fabricated a solar cell using an inkjet-printed PEDOT:PSS hole transport layer [26]. In particular, they observed that the addition of glycerol and surfactant to the PEDOT:PSS inks can improve the surface morphology and conductivity of the thin films. In the same year, *Steirer* et al. developed another solar cell based on an inkjet-printed hole transport layer by investigating the effect of drop spacing and substrate temperature on the quality of the printed thin film [27]. In 2011, *Ely* et al. described an inkjet-printed hole injection/transport layer based on PEDOT:PSS, glycerol, and Triton X-100 [28]. To simulate an OLED pixel structure, an array of SU8 (epoxy-based photoresist) wells was fabricated on indium tin oxide (ITO)/glass substrates, and various surface treatments were tested to control the wetting properties. More recently, *Singh* et al. investigated the effects of substrate surface treatments, drop spacing, and substrate temperature on an inkjet-printed PEDOT:PSS hole transport layer for solar cells [29]. The effect of different organic co-solvents on PEDOT:PSS inkjet printed onto ITO-coated polyethylene terephthalate (PET) substrates was also researched. In particular, diethylene glycol (DEG), triethylene glycol (TRIEG), tetraethylene glycol (Tetra EG), and PEG were used to prepare different formulations [30]. It was observed that the molecular weight, dipole moment, and boiling point of the co-solvents strongly affected the electrical conductivity, morphology, and transparency of the printed thin films. Recently, a hybrid PEDOT:PSS/PEG formulation was used to inkjet print a hole injection layer for OLED devices [8]. Inkjet-printed PEDOT:PSS was also employed as the top transport layer in a solar cell. In this case, because the hole transport layer was deposited on top of an organic layer, it was necessary to properly evaluate the surface energy mismatch and dewetting phenomena. A specific formulation was developed using a combination of solvents and surfactants [31].

Regarding the inkjet printing of highly conductive PEDOT:PSS, different works have been reported in the literature and are summarised in Table S3. In the aforementioned works, the ink optimisation process is often not discussed or only discussed in terms of its effects on the characteristics of the printed film; however, it is not correlated to the rheological and wetting properties of the ink. For this reason, the focus of our work is to determine relationship between the rheological and surface tension characteristics of PEDOT:PSS inks and the macroscopic (coffee ring or dewetting) and microscopic (AFM characterisation) quality of the printed film. In this work, using two commercially available PEDOT:PSS solutions (Clevios™ PH1000 and Clevios™ HIL E 100), we systematically evaluate the effect of co-solvent (ethanol) and surfactant (Triton X-100) quantity on the rheological and surface tension characteristics of the ink, as well as the quality and uniformity of the printed thin film. PH1000, an aqueous PEDOT:PSS solution, is the most commonly used polymeric anode in the optoelectronic field because of its high conductivity and transmittance as a thin film. Indeed, it has been widely and successfully employed as a transparent electrode in OLEDs [32], solar cells [33], and photodiodes [18]. HIL E 100 is a new PEDOT:PSS-based Heraeus formulation; although its conductivity is lower than that of PH1000, it exhibits good hole injection and planarisation properties according to the specifications provided by the producer. Unlike PH1000, it has never been printed and has been rarely employed in optoelectronic devices [34]. Here, for the first time, we report its use as a printed anode deposited using inkjet printing. The morphological, optical, and electrical properties of the optimised printed PEDOT:PSS thin films were evaluated and compared with those of the spin-coated layers. PEDOT:PSS-based films were employed in the fabrication of monochromatic OLEDs to assess their suitability as anodes in optoelectronic devices.

2. Experimental

2.1. Chemicals and reagents

PEDOT:PSS PH1000 and HIL E 100 were purchased from Heraeus Clevios™. Triton X-100, solvents, and all other chemicals were

acquired from Sigma–Aldrich. All chemicals were used as received without further purification.

2.2. Ink and film characterisation

The viscosities of the ink formulations before and after additive-solvent addition were evaluated using a strain-controlled rheometer (Ares, TA Instruments) equipped with parallel plate geometry (diameter = 25 mm). The measurements were performed in steady mode at 20 °C, at shear rates ranging from 10 to 1000 s^{-1}. A CAM 200 (KSV Instruments Ltd., Finland) instrument was used to perform pendant drop measurements to evaluate the surface tension of the solutions. The reported data are the average of three measurements with standard deviations determined from the medium value. The same CAM 200 apparatus was used to perform static contact angle measurements of all solutions by the sessile drop method. Several drops of each solution were deposited onto different areas of the glass substrates and observed for 60 s; their respective averages and standard deviations were then reported. Film thicknesses were measured using a surface profiler (Dektak) characterised by a mechanical stylus with a 12 μm tip diameter. The surface morphologies, including roughness parameters, were characterised using atomic force microscopy (no-contact mode, AFM PARK SYSTEMS XE-100). UV-Vis transmittance measurements were performed using a PerkinElmer UV/Vis/NIR spectrometer (Lambda 1050). PEDOT:PSS conductivity measurements were carried out in a four-point probe configuration at room temperature by applying a direct current of 100 μA. To confirm their reproducibility, we repeated the measurements ten times for each sample.

2.3. OLED fabrication and characterisation

The structure of the fabricated OLEDs consisted of glass/PEDOT:PSS anode/MeO-TPD/CBP:Ir $(ppy)_3$/Bphen/Bphen:Cs/Ag. The glass substrates were cleaned with acetone and isopropyl alcohol for 10 min each and dried with nitrogen. Two different types of high-conductivity PEDOT:PSS (Clevios™ PH1000 and Clevios™ HIL E 100) were used as anodes. PEDOT:PSS layers were printed using a new prototype inkjet printer fabricated by T.P.A. s.r.l. fitted with a single nozzle (diameter = 300 μm). The single nozzle printer moves 1 m/min on a fixed glass substrate and ejects drops (volume = ~15 nL) from a height of 7 mm above the substrate. The individual circular drops were separated by a distance of 1 mm (centre-to-centre). The final printed layers had dimensions of 13 × 24 mm^2. Printed layers were obtained using *the PH1000 #5* and HIL *E #5* inks. The printed layers were dried for 10 min at room temperature, and the sample was then transferred onto a hot plate, which was first heated at 70 °C for 10 min to complete the drying process, and then at 120 °C for 15 min to anneal the PEDOT:PSS. Reference devices with spin-coated PEDOT:PSS anodes were also fabricated. Before spin-coating, plasma oxygen treatment was performed on the glass substrates (50 W, O_2 flow: 30 sccm). Spin-coated PEDOT:PSS thin films were fabricated using two commercially available solutions (*PH1000 #1* and *HIL E #1*), without any modification. Specifically, PH1000 and HIL E were spin-coated at 1000 rpm for 30 s and 800 rpm for 30 s, respectively. Both spin-coated films were then annealed at 120 °C for 15 min.

Subsequently, MeO-TPD (40 nm), CBP:Ir $(ppy)_3$ (25 nm), BPhen (10 nm), BPhen:Cs (40 nm), and Ag (100 nm) were deposited by vacuum thermal evaporation in a Kurt J. Lesker multiple high-vacuum chamber system. The effective light-emitting area of the fabricated device was 15 mm^2. The optoelectronic characteristics of the OLED devices were measured in a glove box using an Optronics OL770 spectrometer coupled to an OL610 telescope unit with an optical fibre for the luminance measurements. The entire system was directly connected by an RS232 cable to a Keithley 2420 current–voltage source meter.

3. Results and discussion

3.1. Formulation and optimisation of inks and thin film formation

The drop formation, printability, and wetting capability of an ink are strongly affected by its physical and chemical properties. In particular, the concentration, viscosity, and surface tension can be modified to optimise the ink formulation. Viscosity values in the range of 5 and 40 cP and surface tension values lower than 40 mN/m are usually considered appropriate for inkjet printing [35,36]. Solvent combinations and additives are the principal elements that can be used to optimise the ink characteristics. Solvents are usually added to adjust the solid content, surface tension, and ink-substrate compatibility. Volatile co-solvents can be used to decrease the drying time. As reported in the introduction, DMSO is specifically used in PEDOT:PSS formulations to improve its conductivity owing to its ability to dissolve insulating PSS shells and induce connections among conductive PEDOT grains. Surfactants further adjust the surface tension and wetting capability of the ink; in fact, owing to their amphiphilic nature, they can easily migrate to any type of surface. Therefore, two commercially available PEDOT:PSS products (Clevios™ PH1000 and Clevios™ HIL E 100) that are usually employed for spin-coating deposition have been modified to develop inkjet-printable formulations and obtain high-quality printed thin films.

The different formulations developed for PH1000-based inks are reported in Table 1. Pristine PH1000 (*PH1000 #1*) has a surface tension of 70 ± 2 mN/m, which is close to that of pure water because it is an aqueous solution. From the rheological curve (Fig. S1a), it is possible to observe a slight shear thinning behaviour for viscosity values ranging from 51 cP at a shear rate of 10 s^{-1} to 16 cP at 1000 s^{-1}, as already reported by Glasser et al. [37]. As previously mentioned, the solid content of *PH1000 #1* is optimised for the spin-coating process, and the solution must be diluted to obtain an inkjet-printed thin film with a thickness and transparency suitable for application as a transparent conductive layer. Moreover, the high solid content of *PH1000 #1* (1–1.3 wt%) causes the rapid clogging of the printer nozzle, limiting the direct deposition of this solution. To overcome this issue, the *PH1000 #2* formulation was developed by adding water to reduce the PEDOT:PSS concentration, DMSO to improve the layer conductivity, and Triton X-100 as a stabilising agent.

PH1000 #2 exhibits a surface tension of approximately 53 ± 2 mN/m (Fig. 1b) and decreased viscosity values compared to *PH1000 #1*, ranging from 6.7 to 3.8 cP at 10 and 1000 s^{-1}, respectively (Fig. S1a), due to the reduction of the solid content in the solution after dilution. From the printing of *PH1000 #2*, we observed a uniform film in the wet state that rapidly recedes during

Table 1
Composition of PH1000 inks with different H_2O and EtOH volume percentages.

Ink	Ink composition (% v/v)				
	PEDOT:PSS	H_2O	DMSO	EtOH	Triton X-100 in H_2O (1.4 mg/mL)
PH1000 #1	100	–	–	–	–
PH1000 #2	14.4	77.5	3.7	–	4.4
PH1000 #3	14.4	63.1	3.7	14.4	4.4
PH1000 #4	14.4	48.7	3.7	28.8	4.4
PH1000 #5	14.4	34.3	3.7	43.2	4.4
PH1000 #6	14.4	19.9	3.7	57.6	4.4
PH1000 #7	14.4	5.4	3.7	72.1	4.4

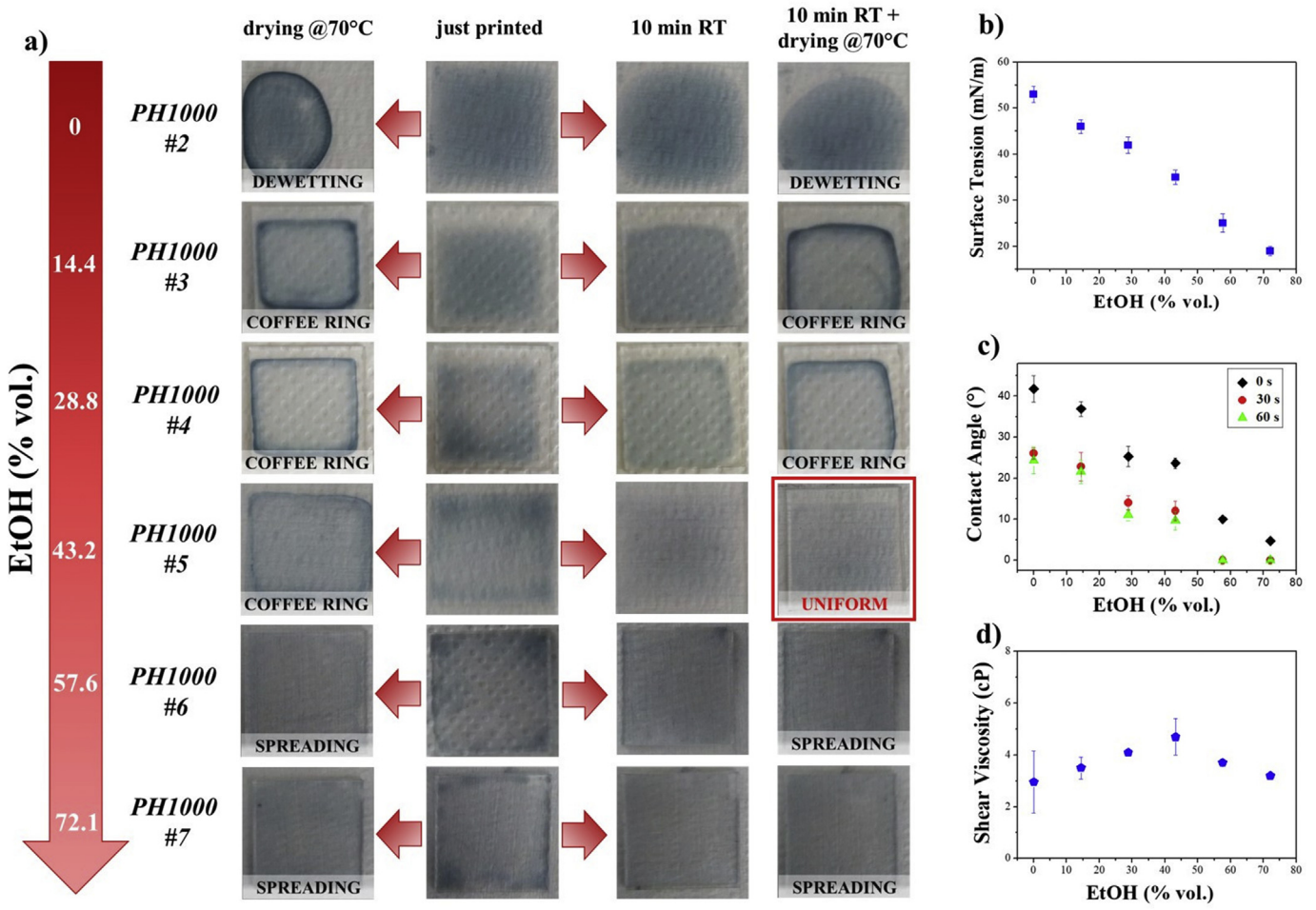

Fig. 1. a) PH1000 #2–#7 film morphology for two different drying processes. b) Surface tension, c) contact angle (at 0, 30 and 60 s) and d) viscosity vs EtOH content (% vol).

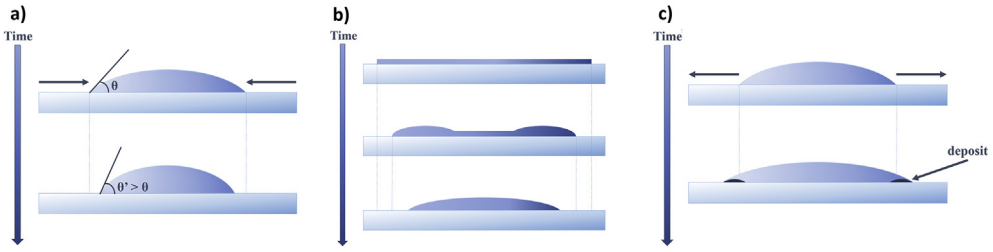

Fig. 2. a) Dewetting of a drop with high surface tension; b) dewetting of a thin film; c) pinning of drop and coffee ring effect.

the drying process (Fig. 1a). This dewetting phenomenon is more evident if the drying phase is performed on a hot plate, and it is likely due to the high surface tension, which is directly related to the "stable" contact angle through Young's equation [21]. In general, when a drop is deposited on a substrate, the surface tension reaches equilibrium, and the drop immediately fixes on the solid, assuming a shape characterised by a contact angle, θ. In a drop with high surface tension (Fig. 2a), the contact line moves inward instead of pinning up on the substrate, causing a reduced and discontinuous thin film deposition. Such an effect is more evident if a large number of drops are placed next to each other—as in the inkjet printing process—to obtain a continuous thin film, which induces the coalescence of the drops that move to the centre of the substrate (Fig. 2b).

To reduce the receding effect and the drying time, ethanol was used as a co-solvent because it has a low surface tension (approximately 22 mN/m) and a lower boiling point (78 °C) than water. In Table 1, the PH1000-based formulations with different volume percentages of water and ethanol are reported. The increase in the ethanol content of the ink (water/ethanol ratio reduction) induces a gradual reduction in the surface tension and contact angle (Fig. 1b and c, respectively), without significantly modifying the rheological behaviour (Fig. S1a) and viscosity values (Fig. 1d) of the inks extrapolated at a high shear rate of 1000 s^{-1} [37]. This means that they are still suitable for inkjet printing deposition. The reduction in the surface tension determines the pinning of the drop to the substrate, with faster evaporation at the contact line than in the central region. This activates a fluid flow from the interior of the

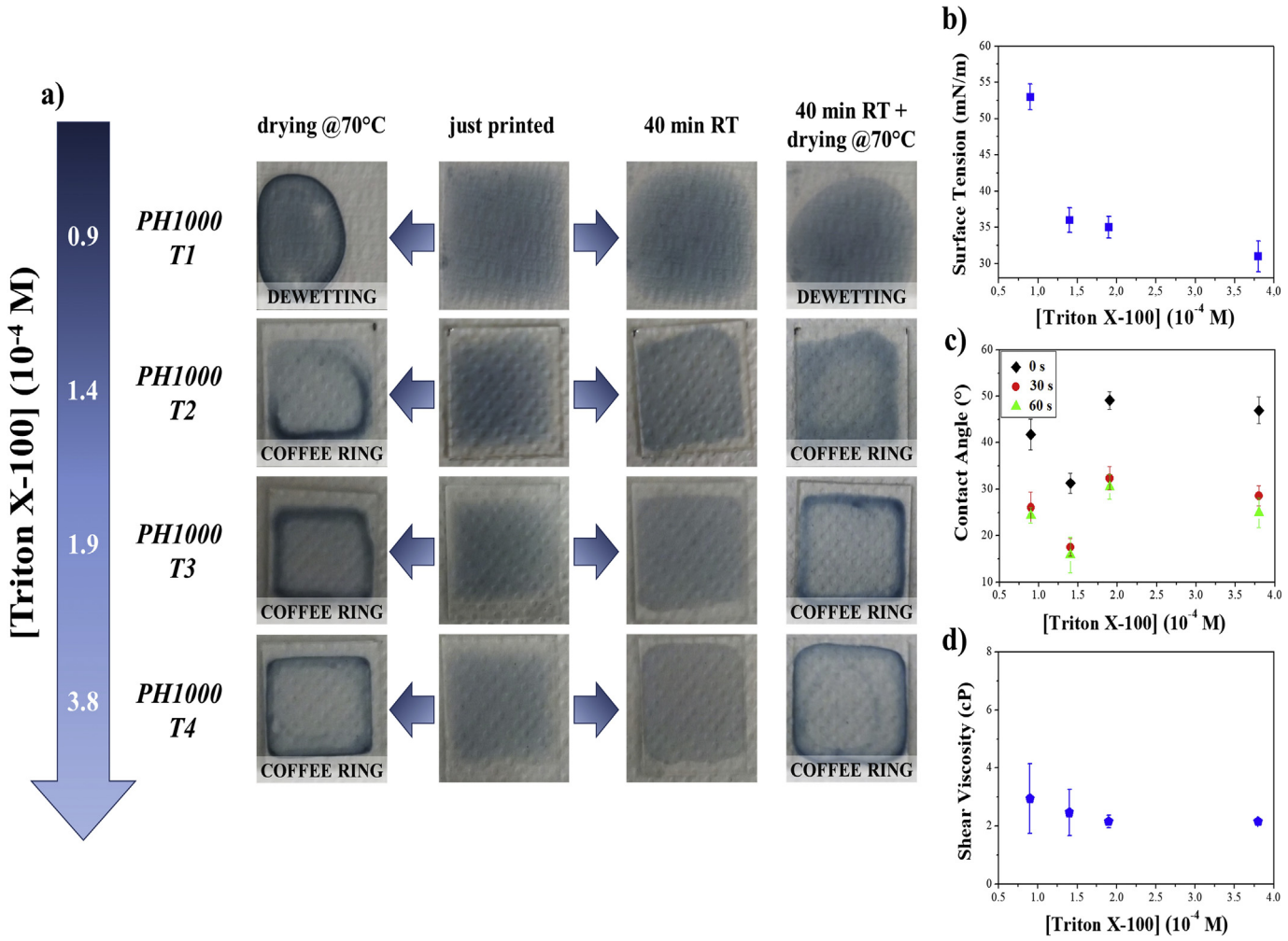

Fig. 3. a) PH1000 T1–T4 film morphology for two different drying processes. b) Surface tension, c) Contact angle (at 0 and 30 s) and d) Viscosity vs [Triton X-100] in the ink (10^{-4} M).

Table 2
Composition of HIL E 100 inks with different H_2O/EtOH volume ratios.

Inks	Ink composition (% v/v)			
	PEDOT:PSS	H_2O	EtOH	Triton X-100 in H_2O (1.4 mg/mL)
HIL E #1	100	–	–	–
HIL E #2	14.4	81.3	–	4.4
HIL E #3	14.4	66.9	14.4	4.4
HIL E #4	14.4	52.5	28.8	4.4
HIL E #5	14.4	38.1	43.2	4.4
HIL E #6	14.4	23.7	57.6	4.4
HIL E #7	14.4	9.2	72.1	4.4

drop to the edge, replenishing the liquid lost due to evaporation. This flow carries the solute particles to the contact line, creating a ring-like morphology and providing the so-called coffee ring effect (Fig. 2c). This effect causes unevenness in inkjet-printed films, and several methods have been proposed to suppress it. In particular, the coffee ring effect can be avoided by weakening the outward flow [38], adding surfactants [39], or exposing the drying drops to the vapours of low-surface-tension liquids [40]. In our case, we observed that the amount of ethanol in the PEDOT:PSS ink formulations is fundamental for reducing the coffee ring effect. When the amount of water was still high, as for *PH1000 #3* (63.1%) and *PH1000 #4* (48.7%), the evaporation rate was low, and the migration of the solute to the edge of the thin film occurred with the formation of the coffee ring (Fig. 1a). The reduction of the water content to 34.3% (*PH1000 #5)* results in the best wetting conditions and a reduced coffee ring effect. In particular, the thin film uniformity was improved by a two-step drying process. First, the sample was left at room temperature for 10 min; this first drying at a low temperature resulted in a slower migration of solute towards the edges, avoiding the coffee ring effect. The sample was then transferred to a hot plate, which was heated at 70 °C for 10 min to complete the drying process, and further heated at 120 °C for 15 min to anneal the PEDOT:PSS (Fig. 1a). If the water content was further decreased, the solution was completely spread on the substrate, and the printing geometry was not retained. The *PH1000 #6* and *PH1000 #7* inks (where % vol. EtOH were 57.6% and 72.1%, respectively) exhibited a contact angle of 0° after only 5 s (Fig. 1c).

These results demonstrate that a uniform thin film is obtained when using an ink with a surface tension value that ensures good wetting characteristics without excessive spreading of the solution (between 30 and 40 mN/m). Moreover, it is important to evaluate the drying process of the wet film; indeed, the use of the right amount (~40%) of low-boiling-point solvent reduces the drying time and improves the thin film quality. For these reasons, *PH1000 #5* ink is the best candidate for the printing of a PEDOT:PSS-based anode layer for OLED applications.

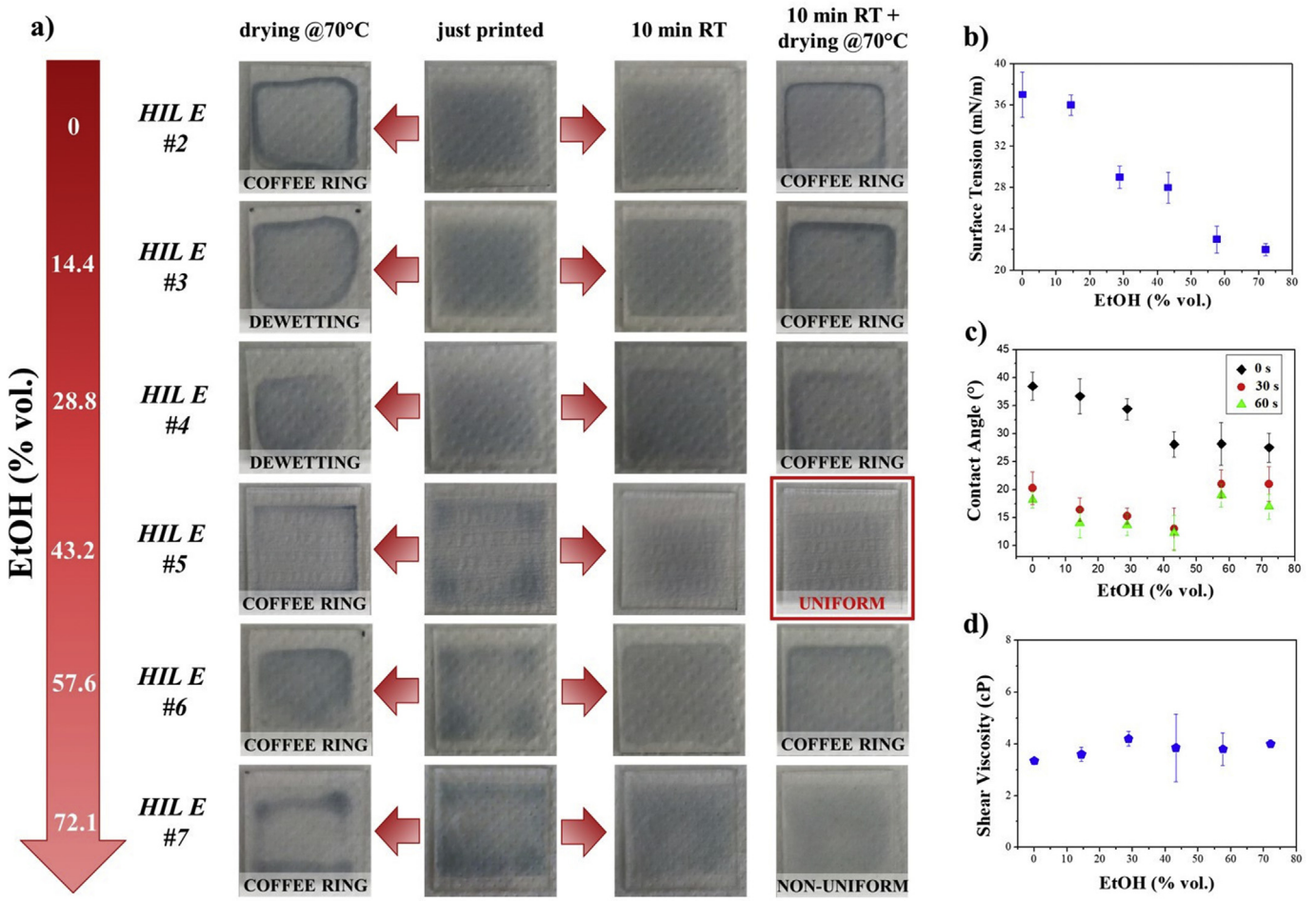

Fig. 4. a) HIL E #2–#7 film morphology for two different drying processes. b) Surface tension, c) contact angle (at 0, 30, and 60 s) and d) viscosity vs EtOH in the ink (% vol).

To further confirm this, we attempted to reduce the surface tension of the ink by adding increasing amounts of surfactant to the formulation, instead of using ethanol as a co-solvent. The prepared formulations are presented in Table S1. As expected, the increase in the surfactant concentration induced a surface tension reduction, reaching almost the same surface tension value as that of *PH1000 #5* (Fig. 3b). As shown in Fig. 3d, the addition of surfactant does not significantly change the viscosity values of the inks extrapolated at a high shear rate of 1000 s^{-1}, so they are still suitable for inkjet printing deposition. Nonetheless, the wetting capability in terms of the contact angle values is not comparable to that of *PH1000 #5* (Fig. 3c). With an increase in surfactant concentration, the contact angle first slightly decreased (*PH1000 T2*) and then tended to increase (*PH1000 T3* and *PH1000 T4*). Furthermore, all the thin films obtained with such formulations showed an evident coffee ring, even when a two-step drying process was employed (Fig. 3a).

The increasing contact angle is due to the critical micelle concentration (CMC). When the surfactant concentration is below the CMC, the surfactant molecules can expose their polar head to the glass substrate and improve the wetting capability of the ink; however, if the surfactant concentration is higher than the CMC, micelle formation occurs, exposing the apolar tail to the substrate, reducing the wetting capability. As a result, there is a threshold value for surfactant addition beyond which the beneficial effect is lost due to the formation of micelles. Moreover, because water is the only solvent in the formulations reported in Table S1, the drying process is excessively slow and the uniformity of the thin films is compromised by the coffee ring effect. These results confirm that both the surface tension and the co-solvent composition of the ink are equally important for obtaining a uniform inkjet-printed thin film.

An ink optimisation process analogous to that used for PH1000 was carried out for the HIL E 100 solution. The ink formulations with different amounts of ethanol are listed in Table 2.

The pristine HIL E 100 aqueous solution (*HIL E #1*) had a surface tension of 32 ± 3 mN/m. In contrast to pure PH1000 (*PH1000 #1*), *HIL E #1* exhibits a very low surface tension compared to that of a typical aqueous solution, likely because surfactants and/or stabilisers are already present in the commercial solution. Regarding the rheological characteristics, *HIL E #1* displayed slight shear thinning behaviour for viscosity values ranging from 30 to 16 cP at 10 and 1000 s^{-1}, respectively (Fig. S2a). As for PH1000, water and ethanol were used in combination to dilute the pristine HIL E 100 solution, and Triton X-100 was added as a surfactant to improve the substrate/ink compatibility and to reduce the nozzle clogging effect. All explored formulations are listed in Table 2. The *HIL E #2* solution showed a surface tension value (37 ± 2 mN/m) higher than that of the pristine solution because it was diluted with water (water surface tension = 70 mN/m). The viscosity value at 1000 s^{-1} decreased to 3.3 cP, owing to the reduction in the solid content of

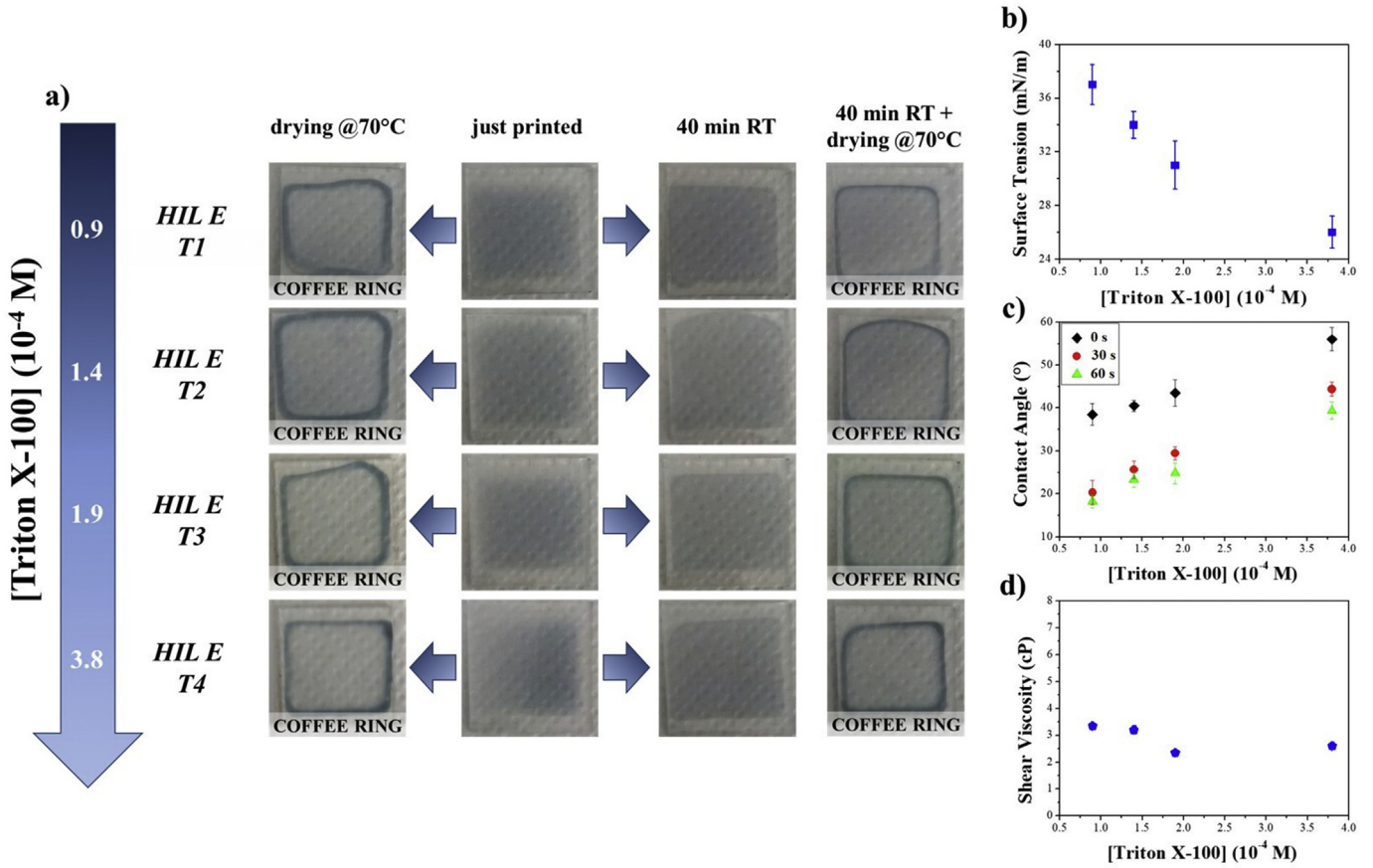

Fig. 5. a) HIL E T1–T4 film morphology for two different drying processes. b) Surface tension, c) contact angle (at 0, 30, and 60 s) and d) viscosity vs [Triton X-100] in the ink (10^{-4}M).

Table 3
Thicknesses, average transmittance between 380 and 780 nm, and conductivities of PH1000 and HIL E 100 films on glass.

Sample		Thickness (nm)	Average transmittance from 380 to 780 nm (%)	Conductivity (S/cm)	Sheet resistance (Ω/sq)	FoM (Figure of Merit)
PH1000 #5	**printed**	250 ± 15	79.1 ± 0.1	676 ± 3	59 ± 4	25.6 ± 2.3
PH1000 #1	**spin-coated**	100 ± 8	83.9 ± 0.1	847 ± 9	118 ± 11	17.4 ± 2.1
HIL E #5	**printed**	550 ± 22	77.6 ± 0.1	23.6 ± 0.4	770 ± 44	1.8 ± 0.1
HIL E #1	**spin-coated**	230 ± 17	83.7 ± 0.1	52.8 ± 0.5	824 ± 69	2.4 ± 0.3

the solution, without modifying the slight shear thinning behaviour (Fig. S2a). In contrast to *PH1000 #2*, the thin film obtained with *HIL E #2* shows a negligible dewetting effect (Fig. 4a) because of the differences in the surface tension values of these two formulations related to the different surface tensions of the pristine solutions (*PH1000 #1* and *HIL E #1*).

The surface tension and contact angle values of *HIL E #2* were sufficient to ensure the wetting of the substrate, but the large quantity of water in the ink induced the formation of the coffee ring (Fig. 4a). As with PH1000, the amount of ethanol was modified to obtain the best ink formulation. With increasing ethanol content, there was a reduction in the surface tension and contact angles (Fig. 4b and c), while the viscosity values at a shear rate of 1000 s^{-1} were comparable (Fig. 4d). In *the HIL E #3* and *HIL E #4* inks, the ethanol quantity was not sufficient to reduce the coffee ring. On the other hand, *the HIL E #5* ink exhibited the smallest contact angle without excessive spreading, and the printed thin film was highly uniform. *HIL E #6* and *HIL E #7*, in which the ethanol content was further increased, showed the same contact angle as that of HIL E #5 at 0 s, while the contact angles at 30 and 60 s were higher, confirming that the best wetting conditions were achieved using *HIL E #5* (Fig. 4c). This difference in behaviour compared to the PH1000 inks is probably due to the interaction between ethanol, Triton X-100, and the stabiliser agents present in *HIL E #1*. Similar to PH1000, we found the ink composition that ensured excellent wetting characteristics and good thin film uniformity without the coffee ring effect (*HIL E #5*).

As was done for PH1000, three new HIL E inks were prepared by increasing the surfactant quantity starting from the *HIL E #2* solution (Table S2). As shown in Fig. 5b and c, although the surface tension decreased with the addition of surfactant, the contact angles increased owing to the formation of micelles. Comparable viscosity values were observed at a shear rate of 1000 s^{-1} by varying the surfactant concentration, as already observed for the other developed formulations (Fig. 5d). The non-ideal wetting conditions, long drying time, and formation of the coffee ring (Fig. 5a) confirm that *HIL E #5* is the best formulation for the inkjet printing of HIL E 100 solution. Considering these results, we focused

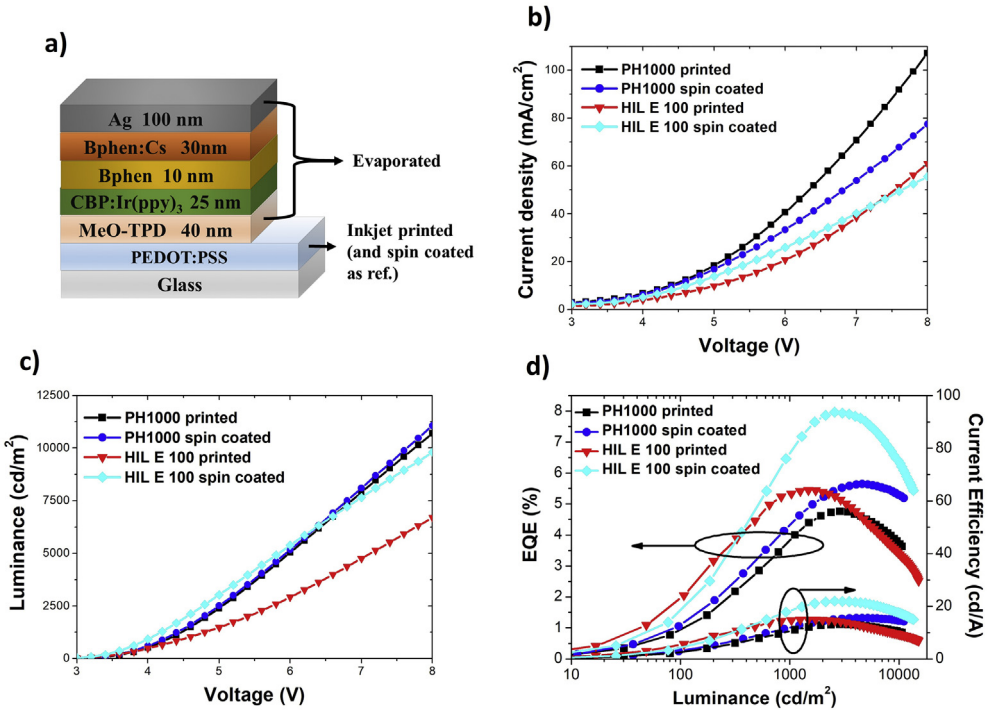

Fig. 6. Characterisation of OLED devices with inkjet-printed PEDOT:PSS (PH1000 #5 and HIL E #5) as anode and spin-coated reference devices. a) Schematic of the device structure; b) current density vs. voltage; c) luminance vs. voltage; and d) efficiency vs. luminance for OLED with PEDOT:PSS deposited by inkjet printing vs spin-coating.

our attention on the characterisation of thin films obtained with the *PH1000 #5* and *HIL E #5* formulations.

3.2. Film characterisation

The thin films obtained by printing *PH1000 #5* and *HIL E #5* inks were characterised to evaluate their suitability as anode layers for bottom-emitting OLED devices. They were also compared with spin-coated thin films fabricated with commercial solutions without any modification (*PH1000 #1* and *HIL E #1*). The three main prerequisites of a thin film to be used as an anode in optoelectronic devices are uniformity with low roughness, transparency, and good electrical conductivity. Atomic force microscopy images of the printed (*PH1000 #5* and *HIL E #5*) and spin-coated PEDOT:PSS (*PH1000 #1* and *HIL E #1*) thin films are shown in Fig. S3. Both PEDOT:PSS typologies exhibit similar low surface roughness to the spin-coated films fabricated as references. In particular, printed *PH1000* is slightly rougher than its spin-coated counterpart (arithmetical mean deviation of the assessed profile (Ra) = 2.7 nm and root mean squared (Rq) = 3.4 nm against Ra = 1.5 nm and Rq = 2.1 nm of the spin-coated film) while the printed *HIL E* is smoother than the spin-coated sample (Ra = 1.8 nm and Rq = 2.3 nm compared to Ra = 1.9 nm and Rq = 2.6 nm, respectively).

Regarding the optical properties of the PEDOT:PSS thin films, the graph in Fig. S4 shows the transmittance spectra in the range of 300–850 nm. Spin-coated layers show higher transmittance compared to printed layers because of their lower thicknesses, as reported in Table 3. Although the printed layers are almost twice as thick as the spin-coated layers, they maintain a high transmittance (close to 80%) and are suitable for application as transparent anodes. Furthermore, the higher thickness values of the printed layers reduces the sheet resistance of the thin film; such thicknesses cannot be attained by the spin-coating process because the deposition speed is already very low (1000 and 800 rpm). Specifically, between 380 and 780 nm, the average transmittance of inkjet-printed PH1000 decreased from 83.9 to 79.1% compared to its spin-coated counterpart, while for HIL E 100 it decreased from 83.7 to 77.6% (Table 3). The electrical conductivity values of the printed and spin-coated thin films were also measured and are presented in Table 3. Spin-coated PH1000 and HIL E 100 have conductivities of 847 ± 9 and 52.8 ± 0.5 S/cm, respectively. Both values were comparable to the conductivities reported by the producer. In contrast, both printed films exhibited lower conductivities. In particular, the conductivity of the printed PH1000 was 676 ± 3 S/cm, while that of HIL E 100 was 23.6 ± 0.4 S/cm. The figure of merit (FoM) is a parameter obtained by the combination of optical and electrical properties ($FoM = \frac{188.5}{\left(\frac{1}{\sqrt{T_{380-780\ nm}}}-1\right)*R_s}$) where $T_{380-780\ nm}$ is the average transmittance from 380 to 780 nm and R_s is the sheet resistance [37], and it is employed to classify thin films for transparent electrode applications. The higher the FoM value, the better the transparent conductor. In this case, printed PH1000 has a higher FoM than its spin-coated counterpart, while the printed HIL E 100 exhibits a slightly lower FoM than that of the spin-coated HIL E 100 (Table 3).

To demonstrate the quality of our printed PEDOT:PSS thin films for electrode applications, Table S3 presents a comparison with some studies where roughness, conductivity, and transparency were evaluated.

3.3. OLED characterisation

OLED devices were fabricated to test the printed PEDOT:PSS thin films as anode layers. The devices consisted of glass/PEDOT:PSS (*PH1000 #5* or *HIL E #5*)/MeO-TPD/CBP:Ir (ppy)$_3$/Bphen/Bphen:Cs/Ag (Fig. 6a). As a reference, OLEDs with spin-coated PH1000 and HIL E 100 (*PH1000 #1* and *HIL E #1*) and ITO were also fabricated.

The current density vs. voltage, luminance vs. voltage, and efficiency vs. luminance curves for the devices with PEDOT:PSS as an

anode are shown in Fig. 6b–d, respectively, while the characteristics of the device with ITO are shown in Fig. S5. The current density values of the devices with PH1000 as the anode layer were higher than those employing HIL E, both for printed and spin-coated anodes, and this is due to the higher conductivity of PH1000. In particular, printed PH1000 shows the highest current density because it has a lower sheet resistance. The luminance values for the device containing PH1000 were also higher than those reported for the device using HIL E. Nevertheless, HIL E-based devices show good luminance values of approximately 10,000 and 7000 cd/m^2 for the spin-coated and printed devices, respectively.

Finally, from Fig. 6d, it appears that OLEDs using HIL E are more efficient than those containing PH1000. In particular, the device with spin-coated HIL E—reaching a maximum external quantum efficiency (EQE) of approximately 8% and a maximum current efficiency (CE) of almost 22 cd/A—is found most efficient. The OLED with printed HIL E reached an EQE of 5.4% and a CE of 15 cd/A. The devices containing PH1000 achieved maximum efficiencies of 5.6% and 15.5 cd/A (spin-coated) and 4.7% and 13.1 cd/A (inkjet-printed). The OLEDs based on HIL E anodes are most efficient because, despite their lower luminance values, they show the lowest current density values. The reported results demonstrate the great potential of the printed PEDOT:PSS-based thin films as transparent electrodes for OLED devices. In particular, the devices based on the HIL E anode exhibit higher efficiencies despite the low electrical conductivity, probably owing to the excellent uniformity and the absence of macroscopic defects.

4. Conclusion

The two high-performance conductive inks (*PH1000 #5* and *HIL E #5*) based on PEDOT:PSS were formulated to successfully deposit transparent and conductive layers for large-scale production. Crucial parameters, such as surface tension, solid content, co-solvents, and ink-substrate interface, were evaluated to obtain the optimal thin film. The combination of water and ethanol as solvents and the use of Triton X-100 as a non-ionic surfactant led to the formation of a uniform thin film while preserving the good rheological properties of the developed inks, making it suitable for inkjet printing. The best wetting conditions were obtained with surface tension values in the range of 28–40 mN/m, but such characteristics are not sufficient to print a high-quality and uniform thin film. The drying phase of the film in the wet state must be sufficiently accelerated by using a low-boiling-point co-solvent (approximately 40 vol.%) to avoid the formation of a coffee ring.

The printed PEDOT:PSS-based thin films show very good morphology, low roughness, and electrical/optical characteristics suitable for transparent conductive layers and for the large-scale production of organic optoelectronic devices. OLEDs with printed PH1000 attained a current density higher than 100 mA/cm^2 at 8 V, luminance higher than 10,000 cd/m^2 at 8 V, and maximum CE of 13.1 cd/A. The OLED device containing HIL E exhibited a lower current density (60 mA/cm^2 at 8 V), luminance of 6700 cd/m^2 at 8 V, and maximum CE close to 15 cd/A, which is comparable to that observed for the corresponding device based on a spin-coated anode. Therefore, the reported ink formulation process is a powerful tool for developing fully printed ITO-free OLEDs.

Declaration of competing interest

The authors declare that they have no known competing financial interests or personal relationships that could have appeared to influence the work reported in this paper.

Acknowledgments

This work was supported by the FISR-CNR national project "TECNOMED - Tecnopolo di nanotecnologia e fotonica per la medicina di precisione" - CUP B83B17000010001, by "TecnoMed Puglia - Tecnopolo per la medicina di Precisione - Regione Puglia" - CUP B84I18000540002, by the MISE project "NANOFAB - Sviluppo di innovative soluzioni tecnologiche di processo per l'uso di nanomateriali per la fabbricazione di tessuti sensorizzati", n. F/030004/02/X28, by the MIUR project "ECOTEC - ECO-sustainable and intelligent fibers and fabrics for TEChnic clothing", PON « R&I» 2014–2020, project N° ARS01_00951, CUP B66C18000300005, and by Regione Puglia, Research for Innovation (REFIN).

Appendix A. Supplementary data

Supplementary data to this article can be found online at https://doi.org/10.1016/j.jsamd.2021.09.001.

Abbreviations

PEDOT:PSS	poly(3,4-ethylenedioxythiophene): poly(styrenesulfonate)
ITO	Indium Tin Oxide
OLED	Organic Light Emitting Diode
EG	Ethylene glycol
DMSO	Dimethyl sulfoxide
DEG	diethylene glycol
TRIEG	triethylene glycol
Tetra EG	tetraethylene glycol
PEG	Polyethylene glycol
CMC	Critical Micellar Concentration
Ra	Arithmetical mean deviation of the assessed profile
Rq	Root mean squared
FoM	Figure of Merit
MeO-TPD	N,N,N′,N′-Tetrakis(4-methoxyphenyl)-4,4′-biphenyldiamine
CBP	4,4-Bis(N-carbazolyl)-1,1-biphenyl
$Ir(ppy)_3$	Tris[2-phenylpyridinato-C2,N]iridium(III)
BPhen	Bathophenanthroline
EQE	External Quantum Efficiency
CE	Current Efficiency
AFM	Atomic Force Microscopy

References

[1] S.-J. Zou, Y. Shen, F.-M. Xie, J.-D. Chen, Y.-Q. Li, J.-X. Tang, Recent advances in organic light-emitting diodes: toward smart lighting and displays, Mater. Chem. Front. 4 (2020) 788–820, https://doi.org/10.1039/C9QM00716D.
[2] Q. Niu, Y. Shao, W. Xu, L. Wang, S. Han, N. Liu, J. Peng, Y. Cao, J. Wang, Full color and monochrome passive-matrix polymer light-emitting diodes flat panel displays made with solution processes, Org. Electron. 9 (2008) 95–100, https://doi.org/10.1016/j.orgel.2007.10.001.
[3] L. Liu, X. Liu, K. Wu, J. Ding, B. Zhang, Z. Xie, L. Wang, Efficient solution-processed blue phosphorescent organic light-emitting diodes with halogen-free solvent to optimize the emissive layer morphology, Org. Electron. 15 (2014) 1401–1406, https://doi.org/10.1016/j.orgel.2014.04.005.
[4] H. Youn, K. Jeon, S. Shin, M. Yang, All-solution blade–slit coated polymer light-emitting diodes, Org. Electron. 13 (2012) 1470–1478, https://doi.org/10.1016/j.orgel.2012.04.008.
[5] S. Khan, L. Lorenzelli, R.S. Dahiya, Technologies for printing sensors and electronics over large flexible substrates: a review, IEEE Sensor. J. 15 (2015) 3164–3185, https://doi.org/10.1109/JSEN.2014.2375203.
[6] M. Singh, H.M. Haverinen, P. Dhagat, G.E. Jabbour, Inkjet printing-process and its applications, Adv. Mater. 22 (2010) 673–685, https://doi.org/10.1002/adma.200901141.
[7] Y.J. Kang, R. Bail, C.W. Lee, B.D. Chin, Inkjet printing of mixed-host emitting layer for electrophosphorescent organic light-emitting diodes, ACS Appl.

Mater. Interfaces 11 (2019) 21784–21794, https://doi.org/10.1021/acsami.9b04675.
[8] C. Feng, X. Zheng, R. Xu, Y. Zhou, H. Hu, T. Guo, J. Ding, L. Ying, F. Li, Highly efficient inkjet printed flexible organic light-emitting diodes with hybrid hole injection layer, Org. Electron. 85 (2020) 105822, https://doi.org/10.1016/j.orgel.2020.105822.
[9] S. Yoon, S. Sohn, J. Kwon, J.A. Park, S. Jung, Double-shot inkjet printing for high-conductivity polymer electrode, Thin Solid Films 607 (2016) 55–58, https://doi.org/10.1016/j.tsf.2016.03.068.
[10] S.I. Na, G. Wang, S.S. Kim, T.W. Kim, S.H. Oh, B.K. Yu, T. Lee, D.Y. Kim, Evolution of nanomorphology and anisotropic conductivity in solvent-modified PEDOT:PSS films for polymeric anodes of polymer solar cells, J. Mater. Chem. 19 (2009) 9045–9053, https://doi.org/10.1039/b915756e.
[11] S. Ashizawa, R. Horikawa, H. Okuzaki, Effects of solvent on carrier transport in poly(3,4-ethylenedioxythiophene)/poly(4-styrenesulfonate), Synth. Met. 153 (2005) 5–8, https://doi.org/10.1016/j.synthmet.2005.07.214.
[12] D. Alemu Mengistie, P.C. Wang, C.W. Chu, Effect of molecular weight of additives on the conductivity of PEDOT:PSS and efficiency for ITO-free organic solar cells, J. Mater. Chem. 1 (2013) 9907–9915, https://doi.org/10.1039/c3ta11726j.
[13] Z. Li, W. Meng, J. Tong, C. Zhao, F. Qin, F. Jiang, S. Xiong, S. Zeng, L. Xu, B. Hu, et al., A nonionic surfactant simultaneously enhancing wetting property and electrical conductivity of PEDOT:PSS for vacuum-free organic solar cells, Sol. Energy Mater. Sol. Cells 137 (2015) 311–318, https://doi.org/10.1016/j.solmat.2015.02.024.
[14] C. Badre, L. Marquant, A.M. Alsayed, L.A. Hough, Highly conductive poly(3,4-ethylenedioxythiophene):Poly (styrenesulfonate) films using 1-ethyl-3-methylimidazolium tetracyanoborate ionic liquid, Adv. Funct. Mater. 22 (2012) 2723–2727, https://doi.org/10.1002/adfm.201200225.
[15] N. Kim, S. Kee, S.H. Lee, B.H. Lee, Y.H. Kahng, Y.R. Jo, B.J. Kim, K. Lee, Highly conductive PEDOT:PSS nanofibrils induced by solution-processed crystallization, Adv. Mater. 26 (2014) 2268–2272, https://doi.org/10.1002/adma.201304611.
[16] J.S. Yeo, J.M. Yun, D.Y. Kim, S.S. Kim, S.I. Na, Successive solvent-treated PEDOT:PSS electrodes for flexible ITO-free organic photovoltaics, Sol. Energy Mater. Sol. Cells 114 (2013) 104–109, https://doi.org/10.1016/j.solmat.2013.02.031.
[17] M. Montanino, G. Sico, C.T. Prontera, A. De Girolamo Del Mauro, S. Aprano, M.G. Maglione, C. Minarini, Gravure printed PEDOT:PSS as anode for flexible ITO-free organic light emitting diodes, Express Polym. Lett. 11 (2017) 518–523, https://doi.org/10.3144/expresspolymlett.2017.48.
[18] M. Schmidt, A. Falco, M. Loch, P. Lugli, G. Scarpa, Spray coated indium-tin-oxide-free organic photodiodes with PEDOT:PSS anodes, AIP Adv. 4 (2014), https://doi.org/10.1063/1.4899044, 0–7.
[19] A. C, B. Luszczynska, B.G.R. Dupont, Z. Sieradzki, Inkjet printing technique and its application in organic light emitting diodes, Disp. Imaging 2 (2017) 339–358.
[20] Z. Du, H. Zhou, X. Yu, Y. Han, Controlling the polarity and viscosity of small molecule ink to suppress the contact line receding and coffee ring effect during inkjet printing, Colloids Surfaces A Physicochem. Eng. Asp. 602 (2020) 125111, https://doi.org/10.1016/j.colsurfa.2020.125111.
[21] H. Yildirim Erbil, Control of stain geometry by drop evaporation of surfactant containing dispersions, Adv. Colloid Interface Sci. 222 (2015) 275–290, https://doi.org/10.1016/j.cis.2014.08.004.
[22] Z. Ding, R. Xing, Q. Fu, D. Ma, Y. Han, Patterning of pinhole free small molecular organic light-emitting films by ink-jet printing, Org. Electron. 12 (2011) 703–709, https://doi.org/10.1016/j.orgel.2011.01.027.
[23] U. Kraft, F. Molina-Lopez, D. Son, Z. Bao, B. Murmann, Ink development and printing of conducting polymers for intrinsically stretchable interconnects and circuits, Adv. Electron. Mater. 6 (2020), https://doi.org/10.1002/aelm.201900681.
[24] J.A. Lim, J.H. Cho, Y.D. Park, D.H. Kim, M. Hwang, K. Cho, Solvent effect of inkjet printed source/drain electrodes on electrical properties of polymer thin-film transistors, Appl. Phys. Lett. 88 (2006), https://doi.org/10.1063/1.2177642.
[25] B. Chen, T. Cui, Y. Liu, K. Varahramyan, All-polymer RC filter circuits fabricated with inkjet printing technology, Solid State Electron. 47 (2003) 841–847, https://doi.org/10.1016/S0038-1101(02)00443-4.
[26] S.H. Eom, S. Senthilarasu, P. Uthirakumar, S.C. Yoon, J. Lim, C. Lee, H.S. Lim, J. Lee, S.H. Lee, Polymer solar cells based on inkjet-printed PEDOT:PSS layer, Org. Electron. 10 (2009) 536–542, https://doi.org/10.1016/j.orgel.2009.01.015.
[27] K.X. Steirer, J.J. Berry, M.O. Reese, M.F.A.M. van Hest, A. Miedaner, M.W. Liberatore, R.T. Collins, D.S. Ginley, Ultrasonically sprayed and inkjet printed thin film electrodes for organic solar cells, Thin Solid Films 517 (2009) 2781–2786, https://doi.org/10.1016/j.tsf.2008.10.124.
[28] F. Ely, C.O. Avellaneda, P. Paredez, V.C. Nogueira, T.E.A. Santos, V.P. Mammana, C. Molina, J. Brug, G. Gibson, L. Zhao, Patterning quality control of inkjet printed PEDOT:PSS films by wetting properties, Synth. Met. 161 (2011) 2129–2134, https://doi.org/10.1016/j.synthmet.2011.08.014.
[29] A. Singh, M. Katiyar, A. Garg, Understanding the formation of PEDOT:PSS films by ink-jet printing for organic solar cell applications, RSC Adv. 5 (2015) 78677–78685, https://doi.org/10.1039/c5ra11032g.
[30] Soleimani-gorgani, A. Co-solvents Roles in PEDOT : PSS Ink-Jet Inks.
[31] S. Kommeren, M.J.J. Coenen, T.M. Eggenhuisen, T.M.W.L. Slaats, H. Gorter, P. Groen, Combining solvents and surfactants for inkjet printing PEDOT:PSS on P3HT/PCBM in organic solar cells, Org. Electron. 61 (2018) 282–288, https://doi.org/10.1016/j.orgel.2018.06.004.
[32] C.T. Prontera, M. Pugliese, R. Giannuzzi, S. Carallo, M. Esposito, G. Gigli, V. Maiorano, Flexible distributed Bragg reflectors as optical outcouplers for OLEDs based on a polymeric anode, J. Infect. Dis. (2020) 1–9, https://doi.org/10.1080/15980316.2020.1825537, 0.
[33] S. Jung, A. Sou, K. Banger, D.H. Ko, P.C.Y. Chow, C.R. McNeill, H. Sirringhaus, All-inkjet-printed, all-air-processed solar cells, Adv. Energy Mater. 4 (2014) 1–9, https://doi.org/10.1002/aenm.201400432.
[34] X. Yin, J. Wang, A. Liu, W. Cai, L. Ying, X. He, Z. Tang, L. Hou, Flexible ITO-free sky-blue polymer light-emitting diodes and printed polymer solar cells based on AgNW/PI transparent conductive electrode, Flex. Print. Electron. 5 (2020) 14003, https://doi.org/10.1088/2058-8585/ab603a.
[35] B. He, S. Yang, Z. Qin, B. Wen, C. Zhang, The roles of wettability and surface tension in droplet formation during inkjet printing, Sci. Rep. 7 (2017) 11841, https://doi.org/10.1038/s41598-017-12189-7.
[36] D. Jang, D. Kim, J. Moon, Influence of fluid physical properties on ink-jet printability, Langmuir 25 (2009) 2629–2635, https://doi.org/10.1021/la900059m.
[37] A. Glasser, É. Cloutet, G. Hadziioannou, H. Kellay, Tuning the rheology of conducting polymer inks for various deposition processes, Chem. Mater. 31 (2019) 6936–6944, https://doi.org/10.1021/acs.chemmater.9b01387.
[38] P.J. Yunker, T. Still, M.A. Lohr, A.G. Yodh, Suppression of the coffee-ring effect by shape-dependent capillary interactions, Nature 476 (2011) 308–311, https://doi.org/10.1038/nature10344.
[39] M. Anyfantakis, Z. Geng, M. Morel, S. Rudiuk, D. Baigl, Modulation of the Co ff ee-ring E ff ect in particle/surfactant Mixtures : the importance of particle – interface interactions, Langmuir 31 (2015) 4113–4120, https://doi.org/10.1021/acs.langmuir.5b00453.
[40] M. Majumder, C.S. Rendall, J.A. Eukel, J.Y.L. Wang, N. Behabtu, C.L. Pint, T.Y. Liu, A.W. Orbaek, F. Mirri, J. Nam, et al., Overcoming the “coffee-stain” effect by compositional marangoni-flow-assisted drop-drying, J. Phys. Chem. B 116 (2012) 6536–6542, https://doi.org/10.1021/jp3009628.